JACS
JOURNAL OF THE AMERICAN CHEMICAL SOCIETY
Article
pubs.acs.org/JACS

Room-Temperature Half-Metallicity in La(Mn,Zn)AsO Alloy via Element Substitutions

Xingxing Li,[†] Xiaojun Wu,[†,‡,§] and Jinlong Yang*[,†,§]

[†]Hefei National Laboratory for Physical Science at the Microscale, [‡]CAS Key Laboratory of Materials for Energy Conversion and Department of Materials Science and Engineering, and [§]Synergetic Innovation Center of Quantum Information & Quantum Physics, University of Science and Technology of China, Hefei, Anhui 230026, China

Supporting Information

ABSTRACT: Exploring half-metallic materials with high Curie temperature, wide half-metallic gap, and large magnetic anisotropy energy is one of the effective solutions to develop high-performance spintronic devices. Using first-principles calculations, we design a practicable half-metal based on a layered La($Mn_{0.5}Zn_{0.5}$)AsO alloy via element substitutions. At its ground state, the pristine La($Mn_{0.5}Zn_{0.5}$)AsO alloy is an antiferromagnetic semiconductor. Either hole doping via (Ca^{2+}/Sr^{2+},La^{3+}) substitutions or electron doping via (H^-/F^-,O^{2-}) substitutions in the $[LaO]^+$ layer induce half-metallicity in the La($Mn_{0.5}Zn_{0.5}$)AsO alloy. The half-metallic gap is as large as 0.74 eV. Monte Carlo simulations based on the Ising model predict a Curie temperature of 475 K for 25% Ca doping and 600 K for 50% H doping, respectively. Moreover, the quasi two-dimensional structure endows the doped La(Mn,Zn)AsO alloy a sizable magnetic anisotropy energy with the magnitude of at least one order larger than those of Fe, Co, and Ni bulks.

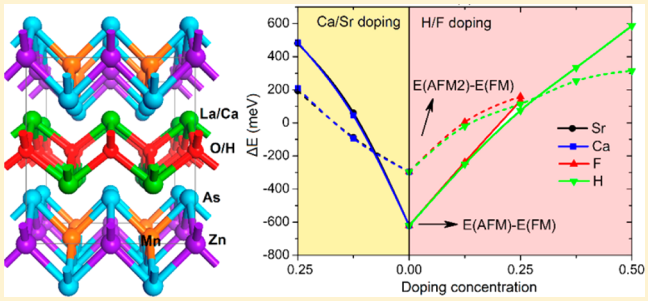

INTRODUCTION

Half-metallic ferromagnets (HMFs),[1] with one spin channel conducting and the other semiconducting, are ideal spintronics materials to provide 100% spin polarized carriers. Until now, various half-metallic compounds have been proposed, such as ternary and quaternary Heusler alloys (NiMnSb, NiCoMnGa, etc.),[1,2] double perovskites (Sr_2FeMoO_6, Sr_2FeReO_6, etc.),[3,4] transition metal pnictides, and chalcogenides in zinc blende phase (CrAs, CrSe, etc.).[5−7] However, to develop practicable spintronic devices with HMFs, some essential issues should be considered. First, the HMFs' Curie temperature should be high enough, that is, notably higher than room temperature. Second, the half-metallic gap should be wide enough to efficiently prevent the spin-flip transition of carriers due to thermal excitation and preserve half-metallicity at room temperature.[8,9] At last, large bulk magnetic anisotropy energy (MAE) is favored in HMFs for their magneto electronics applications. Previously, most theoretically proposed and experimentally synthesized HMFs usually possess some of these three features, and there is still no candidate to fulfill all these requirements.

In this work, we propose a new half-metallic material with high Curie temperature, wide half-metallic gap and a sizable MAE in a ZrCuSiAs-type La($Mn_{0.5}Zn_{0.5}$)AsO alloy via element substitutions. The La($Mn_{0.5}Zn_{0.5}$)AsO alloy possesses a layered structure with magnetic $[(Mn,Zn)As]^-$ layers separated by nonmagnetic $[LaO]^+$ layer, sharing the same "1111" crystal structure as superconducting LaFeAsO.[10] Although it has not been synthesized in experiment, La($Mn_{0.5}Zn_{0.5}$)AsO can be looked as an alloy of two experimentally synthesized rare earth element transition metal arsenide oxides, that is, LaMnAsO[11] and LaZnAsO,[12] which have negligible lattice mismatch (less than 1%) and ideal mutual solubility. In experiment, a possible route to synthesize the La($Mn_{0.5}Zn_{0.5}$)AsO alloy is by mixing La, ZnO:MnO (1:1), and As in a NaCl/KCl flux, followed by an additional annealing procedure.[12] Moreover, an analogous doped system ($La_{1-x}Ba_x$)($Zn_{1-x}Mn_x$)AsO has been synthesized recently.[13]

In our previous study, we have shown that the pristine La($Mn_{0.5}Zn_{0.5}$)AsO alloy is an antiferromagnetic semiconductor with a band gap of 1.3 eV in which the carriers' spin orientation can be controlled by external electric field.[14] Here, we show that the doped alloy with selected element substitutions becomes ideal HMFs with big half-metallic gaps (up to 0.74 eV) and high Curie temperatures. The calculated MAEs are found to be at least 1 order of magnitude larger than those of Fe, Co, and Ni bulks.

COMPUTATIONAL PROCEDURES

Our first-principles calculations are performed by using the density functional theory (DFT) method within the Perdew-Burke-Ernzerhof (PBE) generalized gradient approximation (GGA)[15] implemented in Vienna ab initio Simulation Package (VASP).[16] The strong-correlated correction is considered with

Received: December 3, 2013
Published: March 27, 2014

   dx.doi.org/10.1021/ja412317s | J. Am. Chem. Soc. 2014, 136, 5664−5669

GGA+U method[17] to deal with the Mn's 3d and La's 4f electrons. The effective onsite Coulomb interaction parameter (U) and exchange interaction parameter (J) are set to be 4.0 and 1.0 eV for Mn's 3d electrons, respectively, considering that the Mn atoms in our studied systems are all tetrahedrally coordinated with a nearly d^5 electron configuration, which are very similar to the Mn dopants in III−V and II−VI diluted magnetic semiconductors. In these compounds, the estimated U values for Mn 3d orbitals according to the photoemission spectra vary between 3.5 and 4.5 eV depending on the used theoretical models.[18−21] Thereby, we here take a compromised value of U = 4.0 eV. For La's 4f electrons, we use U = 7.5 eV and J = 1.0 eV.[22] We do not apply the strong-correlated correction on Zn atoms due to their 3d orbitals being fully occupied and far away from the Fermi level in our systems. Note that it is not necessary to add electron correlation for La^{3+} due to the absence of 4f and 5d electrons. Our test calculations with U_{4f} = 0, 4.5, and 7.5 eV present similar density of states (DOS) at the Fermi energy level. There is only difference in the DOS above the Fermi energy level with different values of U_{4f}. The projector augmented wave (PAW) potential[23] and the plane-wave cutoff energy of 400 eV are used. A 2 × 2 × 1 supercell is employed with a Monkhorst−Pack k-point mesh of 7 × 7 × 5. Test calculations show that the PBE method predicts well on the lattice constant, whereas underestimates the band gap. For example, the lattice constant of LaMnAsO optimized by PBE is $a = b$ = 4.093 Å, c = 9.016 Å, matching very well with the experimental value ($a = b$ = 4.124 Å, c = 9.030 Å),[11] whereas PBE+U predicts a lattice constant 0.10 and 0.22 Å larger than that of PBE for a/b and c, respectively. The calculated band gap of LaMnAsO with PBE method is 0.43 eV, which is greatly underestimated compared to the experimental result (∼1.4 eV).[24] The PBE+U method presents an improved value (∼1.06 eV). Thus, in the following calculations, the cell shape, cell volume and the positions of all atoms are relaxed without symmetry constraints with PBE functional. The electronic and magnetic properties are computed with PBE +U functional. The criterion for the total energy and force is set as 1 × 10^{-6} eV and 0.01 eV/Å, respectively. Magnetic anisotropy energies are calculated with an energy cutoff energy of 500 eV and convergence of 1 × 10^{-7} eV for total energy.

RESULTS AND DISCUSSION

The optimized structure of pristine $La(Mn_{0.5}Zn_{0.5})AsO$ alloy is shown in Figure 1a, which features a layered structure with $[LaO]^+$ layers and $[(Mn,Zn)As]^-$ layers stacked in an AB sequence. Chemical bonding within the layers possesses tetrahedral coordination patterns with predominantly covalent character and the interlayer bonding is mainly of an ionic type. Due to the strong ionic-type interaction between $[LaO]^+$ and $[(Mn,Zn)As]^-$ layers, it is expected the electron/hole doping in the nonmagnetic $[LaO]^+$ layer will affect the charge status of the magnetic $[(Mn,Zn)As]^-$ layer via charge transfer between them. Therefore, the magnetic behavior of the $[(Mn,Zn)As]^-$ layer, for example, transition from antiferromagnetic to ferromagnetic coupling, can be tuned.

For this purpose, the substitution of La^{3+}/O^{2-} with heterovalent atoms was considered in the $[LaO]^+$ layer. We use divalent Ca or Sr atoms to replace trivalent La atoms to introduce holes in the system, while electrons are doped by substitution of O with univalent H or F atoms. The solubility of selected atoms in the $La(Mn_{0.5}Zn_{0.5})AsO$ alloy may be a technique problem in reality. Note, the Ca/Sr doping is a

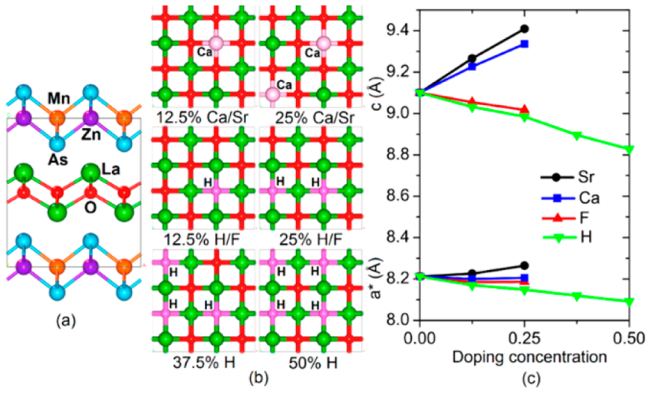

Figure 1. (a) Structure of pristine $La(Mn_{0.5}Zn_{0.5})AsO$ alloy. (b) Models of the $[LaO]^+$ layer with $(Ca^{2+}/Sr^{2+},La^{3+})$ and $(H^-/F^-,O^{2-})$ substitutions at different concentrations. (c) Optimized lattice constants of the doped $La(Mn_{0.5}Zn_{0.5})AsO$ alloy, where $a^* = (a + b)/2$.

widely used technique in Manganite perovskites such as $LaMnO_3$ for the study of colossal magnetoresistance.[25] The upper limit of doping concentration of Sr in $La_{1-x}Sr_xMnO_3$ could reaches x = 0.6,[26] while Ca is soluble in $LaMnO_3$ at arbitrary concentrations.[27] Thus, the mutual solubility between Ca^{2+}/Sr^{2+} and La^{3+} will not be a technique problem in our systems. Upon the F and H doping, the poor solubility is observed in previous reported $LaFeAsO_{1-x}F_x$,[10] which induces novel superconductivity, whereas the doping concentration of H can reach to x = 0.53 in $LaFeAsO_{1-x}H_x$.[28] Later on, a higher concentration of x = 0.73 is achieved in $LaMnAsO_{1-x}H_x$,[29] which directly demonstrates the possibility of high solubility of H atom in $La(Mn_{0.5}Zn_{0.5})AsO$ alloy.

In this work, doping concentrations of 0.125 and 0.25 for Ca/Sr and F doping, and 0.125, 0.25, 0.375, and 0.5 for H doping are considered in the following calculations. The substitution models are shown in Figure 1b. Different doping configurations were considered, and we found that H atoms prefer to stay at next-nearest O sites, while Ca atoms favor next-next-nearest La sites (see Figure S1 in the Supporting Information). Further, test calculations also show that the distribution of introduced atoms does not affect the electronic properties of the alloy too much. As shown in Figure S2 in the Supporting Information, the density of states (DOS) profiles for 25% Ca/H doping with different substitution patterns are found to be very similar.

The element substitutions also induce a remarkable distortion in the z-direction compared to that in the xy-plane in the doped $La(Mn_{0.5}Zn_{0.5})AsO$ alloy, as shown in Figure 1c. The $(Ca^{2+}/Sr^{2+},La^{3+})$ substitution induces an expansion of the lattice while a shrinkage effect occurs for $(H^-/F^-,O^{2-})$ substitution. There is no notable change in the cell shape after fully relaxation on both cell and atomic position except 12.5% $(Ca^{2+}/Sr^{2+},La^{3+})$ substitution. For the latter, the difference value between lattice constants a and b is about 0.05 Å. Test optimizations with PBE+U method present similar result. This is because that we used the ground stripe-type antiferromagnetic (AFM) coupling state (AFM2 state in Figure 2a) when performing cell optimization, which breaks the symmetry between a-axis and b-axis. The optimization at its ferromagnetic (FM) state removes the difference between the values of lattice constants a and b.

dx.doi.org/10.1021/ja412317s | J. Am. Chem. Soc. 2014, 136, 5664−5669

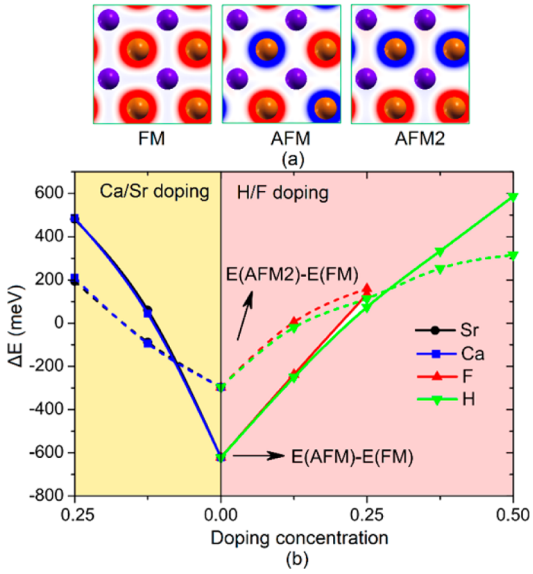

Figure 2. (a) Distribution of spin density in $[(Mn,Zn)As]^{-}$ layer for $(La_{0.75}Ca_{0.25})(Mn_{0.5}Zn_{0.5})AsO$ under ferromagnetic (FM), antiferromagnetic (AFM), and stripe-type antiferromagnetic (AFM2) states with the isovalue of 0.05e/Å^3. Red and blue indicate the positive (spin up) and negative (spin down) values, respectively. (b) Dependence of relative stabilities between FM, AFM states (solid lines), and FM, AFM2 states (dashed lines) on doping concentrations for Ca/Sr doping and H/F doping.

For all the doped $La(Mn_{0.5}Zn_{0.5})AsO$ alloys, the magnetic moments mainly localize on Mn atoms in the $[(Mn,Zn)As]^{-}$ layer, as illustrated in Figure 2a. To find the preferred magnetic coupling in the doped $La(Mn_{0.5}Zn_{0.5})AsO$ alloys, the FM, AFM, as well as a special stripe-type AFM state (AFM2) were considered. Previously, the stripe-type antiferromagnetic coupling has been discovered as ground state in the iron-based superconductor LaFeAsO.[30] The magnetic coupling order between neighboring $[(Mn,Zn)As]^{-}$ layers are not studied, since the interlayer distance between two $[(Mn,Zn)As]^{-}$ layers is about 9 Å and the interlayer magnetic coupling is weak. In our calculations, the interlayer magnetic coupling is set to be FM based on previous experiments.[31,32]

To clarify the dependence of magnetic coupling on the substitution, we plot the variation of exchange energies with the increasing doping concentrations in Figure 2b, which is defined as energy differences between AFM and FM states. The pristine $La(Mn_{0.5}Zn_{0.5})AsO$ alloy exhibits stable AFM coupling with a large exchange energy at its ground state. Both $(Ca^{2+}/Sr^{2+},La^{3+})$ and $(H^{-}/F^{-},O^{2-})$ substitutions induce a magnetic transition from AFM coupling to FM coupling in the alloy. The critical point occurs at a lower concentration for hole-type $(Ca^{2+}/Sr^{2+},La^{3+})$ substitutions than that in the electron-type $(H^{-}/F^{-},O^{2-})$ substitutions, indicating that the hole doping is more efficient in gaining ferromagnetism. Moreover, the $(Ca^{2+}/Sr^{2+},La^{3+})$ substitution with a concentration of 12.5% also induces a magnetic transition from AFM coupling to stripe-type AFM2 coupling before the AFM-FM transition. At 25% Ca/Sr doping and 50% H doping, the doped systems possess robust ferromagnetic ground state with large values of exchange energies (over 400 meV per supercell) comparable to that of pristine $La(Mn_{0.5}Zn_{0.5})AsO$.

To develop a practicable spintronic device, the Curie temperatures (T_c) of materials should be comparable to or higher than room temperature. Here, we adopt the Ising model to evaluate the magnetic exchange parameters and the mean field theory (MFT) to estimate the Curie temperatures of the doped $La(Mn_{0.5}Zn_{0.5})AsO$ alloy.[33,34] Counting in the next-nearest magnetic exchange interaction, the Hamiltonian can be written as eq 1, where J_1 and J_2 are the nearest and next-nearest exchange parameters, M_i is the magnetic moment at sites i, (i,j) and (k,l) are nearest site pairs and next-nearest site pairs, respectively.

$$H = -\sum_{i,j} J_1 M_i \cdot M_j - \sum_{k,l} J_2 M_k \cdot M_l \quad (1)$$

For the doped $La(Mn_{0.5}Zn_{0.5})AsO$ alloy, the magnetic Mn atoms form a simple square lattice (Figure 3a) with M = 4.5

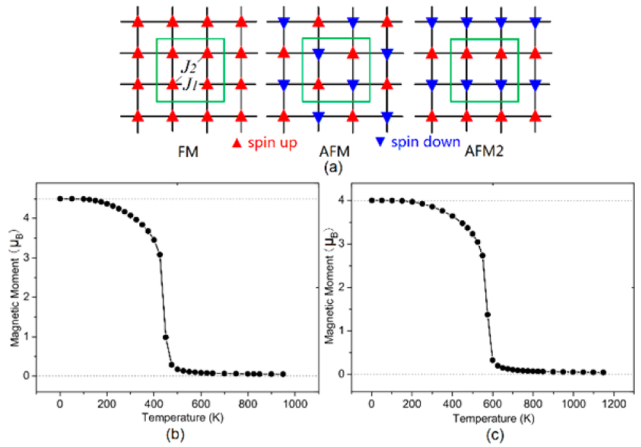

Figure 3. (a) Ising model considering both nearest and next-nearest exchange interactions. Each lattice point represents a magnetic Mn atom. Variation of the magnetic moment per unit cell with respect to temperature for (b) $(La_{0.75}Ca_{0.25})(Mn_{0.5}Zn_{0.5})AsO$ and (c) $La(Mn_{0.5}Zn_{0.5})As(O_{0.5}H_{0.5})$ respectively.

and 4.0 μB for 25% Ca doping and 50% H doping, respectively. The magnetic energies of the 2 × 2 × 1 supercell under FM, AFM, and AFM2 states can be evaluated by eqs 2−4. Then with the AFM − FM energy difference calculated by VASP, the exchange parameters J_1 and J_2 are obtained according to eqs 5 and 6.

$$E(\mathrm{FM}) = -8(J_1 + J_2)M^2 \quad (2)$$

$$E(\mathrm{AFM}) = 8(J_1 - J_2)M^2 \quad (3)$$

$$E(\mathrm{AFM2}) = 8J_2M^2 \quad (4)$$

$$J_1 = [E(\mathrm{AFM}) - E(\mathrm{FM})]/16M^2 \quad (5)$$

$$J_2 = \frac{[2(E(\mathrm{AFM2}) - E(\mathrm{FM})) - (E(\mathrm{AFM}) - E(\mathrm{FM}))]}{32M^2} \quad (6)$$

The calculated exchange parameters are J_1 = 1.50 meV, J_2 = −0.10 meV and J_1= 2.29 meV, J_2= 0.09 meV for $(La_{0.75}Ca_{0.25})(Mn_{0.5}Zn_{0.5})AsO$ and $La(Mn_{0.5}Zn_{0.5})As(O_{0.5}H_{0.5})$, respectively. In the following, the partition function of each magnet with an integer magnetic moment M can be obtained with eq 7, where γ_1 = 4, γ_2 = 4 are the nearest and next-nearest coordination numbers of the Mn atoms, respectively. The ensemble-average magnetic moment $\langle M \rangle$ can be calculated with eq 8, where the

dx.doi.org/10.1021/ja412317s | J. Am. Chem. Soc. 2014, 136, 5664−5669

$\langle M\rangle$ changes with the parameter $p = (\gamma_1 J_1 + \gamma_2 J_2)/k_B T$, and the critical point p_c corresponds to the Curie temperature T_c. The values of p_c are calculated to be 3/35, 1/8, and 1/5 for M = 5.0, 4.0, and 3.0 μ_B, respectively. At 25% Ca doping, the local magnetic moment is M = 4.5 μ_B and the Curie temperature is estimated to be 612 K < T_c < 656 K. In the case of 50% H doping, the local magnetic moment is M = 4.0 μ_B and the Curie temperature is predicted to be T_c = 884 K.

$$Z = \sum_{m=-M,-M+2,\ldots,M-2,M} e^{(\gamma_1 J_1+\gamma_2 J_2)m\langle M\rangle/k_B T} \quad (7)$$

$$\langle M\rangle = \frac{1}{Z}\sum_{m=-M,-M+2,\ldots,M-2,M} m \times e^{(\gamma_1 J_1+\gamma_2 J_2)m\langle M\rangle/k_B T} \quad (8)$$

It is well-known that the Curie temperature T_c predicted by MFT is probably overestimated. We performed Monte Carlo (MC) simulations of the magnetic moment as a function of temperature to obtain the precise value of T_c. The MC simulations last for 1×10^5 loops with an (80×80) supercell. In each loop, the spins on all the magnetic sites flip randomly. Larger supercells or longer loops have been tested to give very similar results. From Figure 3b, it can be seen that, for $(La_{0.75}Ca_{0.25})(Mn_{0.5}Zn_{0.5})AsO$, the magnetic moment per unit cell starts dropping gradually from 4.5 μ_B at about 200 K, then the paramagnetic state is achieved at a temperature of about 475 K. For $La(Mn_{0.5}Zn_{0.5})As(O_{0.5}H_{0.5})$, the Curie temperature is predicted to be 600 K (Figure 3c). Compared to the MFT, the Curie temperature is reduced by 23% and 32% for $(La_{0.75}Ca_{0.25})(Mn_{0.5}Zn_{0.5})AsO$ and $La(Mn_{0.5}Zn_{0.5})As(O_{0.5}H_{0.5})$, respectively. Note that if other models are used, the results can be different. A test calculation based on the classical Heisenberg Hamiltonian is also performed,[35] and the predicted T_c are about 300 and 550 K for $(La_{0.75}Ca_{0.25})(Mn_{0.5}Zn_{0.5})AsO$ and $La(Mn_{0.5}Zn_{0.5})As(O_{0.5}H_{0.5})$, respectively (see Figure S3 in the Supporting Information). Considering this model tends to underestimate the Curie temperature,[35] the results are in good accordance with those based on the Ising model.

The DOSs of the doped alloys are calculated further to understand their electronic properties. Figure 4a and d shows the calculated DOSs of $(La_{0.75}Ca_{0.25})(Mn_{0.5}Zn_{0.5})AsO$ and $La(Mn_{0.5}Zn_{0.5})As(O_{0.5}H_{0.5})$, respectively. Clearly, both $(La_{0.75}Ca_{0.25})(Mn_{0.5}Zn_{0.5})AsO$ and $La(Mn_{0.5}Zn_{0.5})As(O_{0.5}H_{0.5})$ are half-metals, exhibiting complete spin-polarization at the Fermi level. The half-metallic gaps (labeled as δ in Figure 4a and d) are 0.74 and 0.46 eV, comparable to those of double perovskites Sr_2FeMoO_6, Sr_2FeReO_6 (about 0.5 eV),[3,4] transition metal pnictides, and chalcogenides (up to 0.88 eV).[6] A large half-metallic gap can efficiently prevents the spin flip transitions in HMFs which may occur far below T_c and thus enhance the stability of their half-metallicity. The HSE06 hybrid functional[36,37] was also used to confirm the PBE+U calculations (see Figure S4 in the Supporting Information). The doped La(Mn,Zn)AsO are still half-metals. The calculated half-metallic gaps are 1.36 and 0.55 eV for $(La_{0.75}Ca_{0.25})(Mn_{0.5}Zn_{0.5})AsO$ and $La(Mn_{0.5}Zn_{0.5})As(O_{0.5}H_{0.5})$ respectively, larger than those with PBE+U.

In $(La_{0.75}Ca_{0.25})(Mn_{0.5}Zn_{0.5})AsO$, the states around the Fermi level are mainly contributed by As and Mn atoms, as shown in Figure 4b. The orbital-projected DOS, shown in Figure 4c, indicates that these states mainly come from As's 4p and Mn's 3d orbitals. The strong hybridization between them reveals that the ferromagnetism originates from the Zener's p−d exchange interaction.[38,39] A weak p−d hybridization can be also observed in $La(Mn_{0.5}Zn_{0.5})As(O_{0.5}H_{0.5})$, as shown in Figure 4e and f. This may be the reason why the electron doping is less efficient than hole doping to induce the AFM-FM transition in $La(Mn_{0.5}Zn_{0.5})AsO$.

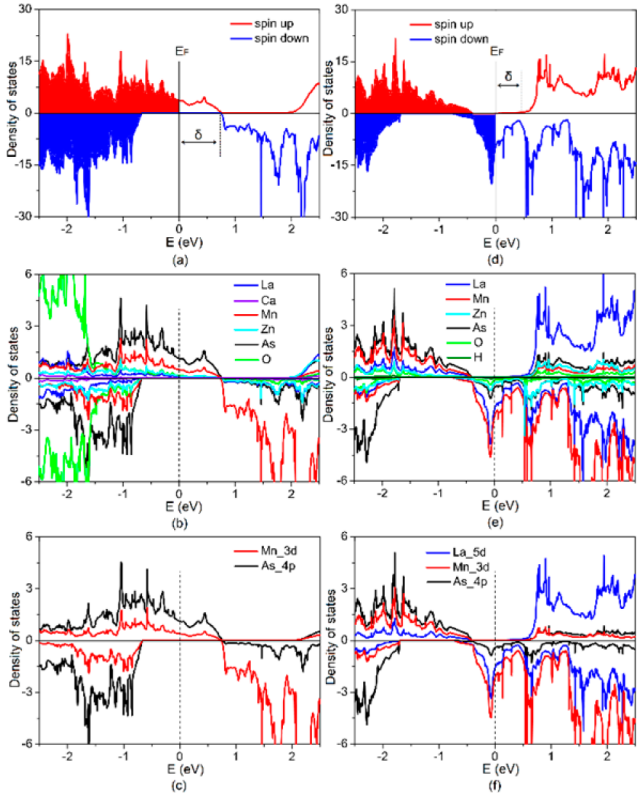

Figure 4. (a) Total density of states, (b) atom-projected density of states, and (c) orbital-projected density of states for $(La_{0.75}Ca_{0.25})(Mn_{0.5}Zn_{0.5})AsO$. (d), (e), and (f) for $La(Mn_{0.5}Zn_{0.5})As(O_{0.5}H_{0.5})$, respectively. The Fermi levels are all set to zero.

In both $(La_{0.75}Ca_{0.25})(Mn_{0.5}Zn_{0.5})AsO$ and $La(Mn_{0.5}Zn_{0.5})As(O_{0.5}H_{0.5})$, there is no sharp impurity state peak that comes from Ca or H atom around the Fermi level, indicating that the impurity states are not localized at the doping sites. From the atom-projected DOS, it can be seen that the introduced holes mainly locate on the As atoms, while the doped electrons mostly reside at Mn, La atom sites. This is further confirmed by bader charge analysis[40] (see Table S1 in the Supporting Information). The interlayer charge transfer is 0.12 hole/electron per chemical formula for 25% Ca doping and 50% H doping, respectively. The excess carriers in the $[(Mn,Zn)As]^-$ layer lead to the rise of carrier-mediated ferromagnetic exchange interaction and the Zener's p−d exchange interaction, which exceeds the antiferromagnetic superexchange interaction and results in the transition of antiferromagnetic spin order to ferromagnetic spin order.[14]

MAE is also an important property for magnetic materials which determines the low-temperature orientation of the magnetization with respect to the lattice structure. It is directly related to the thermal stability of recorded data in magnetic or magneto-optic data storage, and to reduce the used grain size per bit of information requires an increased MAE per atom. It is known that reduced dimensionality and symmetry would result MAE several orders of magnitude larger than that of bulk systems.[41,42] Due to its intrinsic quasi two-dimensional

dx.doi.org/10.1021/ja412317s | J. Am. Chem. Soc. 2014, 136, 5664−5669

structure, a sizable MAE is expected in the doped La($Mn_{0.5}Zn_{0.5}$)AsO alloy.

With spin−orbit coupling (SOC) calculations, the relative stabilities along three magnetization directions, that is, (001), (100), and (110), are studied and the easy axis (EA) is determined for ($La_{0.75}Ca_{0.25}$)($Mn_{0.5}Zn_{0.5}$)AsO and La($Mn_{0.5}Zn_{0.5}$)As ($O_{0.5}H_{0.5}$), together with LaMnAsO to verify the accuracy of our calculations, as summarized in Table 1. The

Table 1. Summary of Magnetic Anisotropy Energy in μeV/Mn and the Easy Axis (EA) for LaMnAsO, ($La_{0.75}Ca_{0.25}$)($Mn_{0.5}$ $Zn_{0.5}$)AsO, and La($Mn_{0.5}Zn_{0.5}$)As($O_{0.5}H_{0.5}$)

	$E(100) - E(001)$	$E(110) - E(001)$	EA
LaMnAsO	72	72	(001)
($La_{0.75}Ca_{0.25}$)($Mn_{0.5}Zn_{0.5}$)AsO	−498	−509	(110)
La($Mn_{0.5}Zn_{0.5}$)As($O_{0.5}H_{0.5}$)	−191	−200	(110)

easy axis of LaMnAsO is along (001) direction, that is, parallel to the *c*-axis, consistent well with the experiments.[31,32] With doping, The easy axis in LaMnAsO rotates from the *c*-axis to the *a*,*b*-plane in ($La_{0.75}Ca_{0.25}$)($Mn_{0.5}Zn_{0.5}$)AsO and La($Mn_{0.5}Zn_{0.5}$)As($O_{0.5}H_{0.5}$). The calculated MAEs are −0.51 and −0.20 meV/Mn for ($La_{0.75}Ca_{0.25}$)($Mn_{0.5}Zn_{0.5}$)AsO and La($Mn_{0.5}Zn_{0.5}$)As($O_{0.5}H_{0.5}$), respectively. These values are about one to 2 orders of magnitude larger than those of Fe (−1.4 μeV per atom), Co (−65 μeV per atom), and Ni (2.7 μeV per atom) bulks.[43,44] Moreover, the magnitude of calculated MAEs are comparable to those of monolayer of Fe, Co deposited on Rh(111) and Pt(111) substrates. For example, the values are 0.08, −0.37, 0.10, and 0.15 meV per metal atom for Fe/Rh(111), Co/Rh(111), Fe/Pt(111), and Co/Pt(111) systems, respectively.[45,46] The large bulk MAE makes our systems promising for magneto electronics applications. To our knowledge, such large bulk MAE has rarely been reported in other half-metallic systems from traditional three-dimensional HMFs to low-dimensional HMFs.[47]

CONCLUSIONS

In summary, we presented a new type of HMF of the doped La(Mn,Zn)AsO alloy with high Curie temperature, wide half-metallic band gap, and sizable magnetic anisotropy energy for practical applications in spintronics. Either the hole-type (Ca^{2+}/Sr^{2+},La^{3+}) substitutions or electron-type (H^-/F^-,O^{2-}) substitutions induce AFM−FM and semiconductor−HMF transitions in the alloy. The half-metallic La(Mn,Zn)AsO with element substitution possesses both wide half-metallic gaps (up to 0.74 eV) and high Curie temperature ranging from 475 K for 25% Ca doping to 600 K for 50% H doping. Moreover, a sizable bulk MAE is found under both types of doping with the values comparable to those of a surface-deposited transition metal monolayer.

Our proposed system belongs to the big family of "1111" ZrCuSiAs-type compunds, and it is expected that, by similar design, other half-metallic systems can be obtained with attractive electronic and magnetic properties, providing great opportunities for spintronics and electronics devices.

ASSOCIATED CONTENT

Supporting Information

Three different patterns of substitution for 25% H doping and 25% Ca doping, and corresponding density of states; the Monte Carlo simulations based on the classical Heisenberg Hamiltonian; the calculated density of states with HSE06 functional; the bader charge analysis. This material is available free of charge via the Internet at http://pubs.acs.org.

AUTHOR INFORMATION

Corresponding Author

jlyang@ustc.edu.cn

Notes

The authors declare no competing financial interest.

ACKNOWLEDGMENTS

This work is partially supported by the National Key Basic Research Program (2011CB921404, 2012CB922001), by NSFC (21121003, 91021004, 20933006, 11004180, 51172223), by Strategic Priority Research Program of CAS (XDB01020300), by Fundamental Research Funds for the Central Universities (WK2060140014, WK2060190025), and by USTCSCC, SCCAS, Tianjin, and Shanghai Supercomputer Centers.

REFERENCES

(1) de Groot, R. A.; Mueller, F. M.; Vanengen, P. G.; Buschow, K. H. J. *Phys. Rev. Lett.* **1983**, *50*, 2024−2027.

(2) Alijani, V.; Winterlik, J.; Fecher, G. H.; Naghavi, S. S.; Felser, C. *Phys. Rev. B* **2011**, *83*, 184428.

(3) Kobayashi, K. I.; Kimura, T.; Sawada, H.; Terakura, K.; Tokura, Y. *Nature* **1998**, *395*, 677−680.

(4) Kobayashi, K. I.; Kimura, T.; Tomioka, Y.; Sawada, H.; Terakura, K.; Tokura, Y. *Phys. Rev. B* **1999**, *59*, 11159−11162.

(5) Galanakis, I.; Mavropoulos, P. *Phys. Rev. B* **2003**, *67*, 104417.

(6) Xie, W. H.; Xu, Y. Q.; Liu, B. G.; Pettifor, D. G. *Phys. Rev. Lett.* **2003**, *91*, 037204.

(7) Liu, B. G. *Lect. Notes Phys.* **2005**, *676*, 267−291.

(8) Fong, C. Y.; Qian, M. C.; Liu, K.; Yang, L. H.; Pask, J. E. *J. Nanosci. Nanotechnol.* **2008**, *8*, 3652−3660.

(9) Hordequin, C.; Ristoiu, D.; Ranno, L.; Pierre, J. *Eur. Phys. J. B* **2000**, *16*, 287.

(10) Kamihara, Y.; Watanabe, T.; Hirano, M.; Hosono, H. *J. Am. Chem. Soc.* **2008**, *130*, 3296−3297.

(11) Nientiedt, A. T.; Jeitschko, W.; Pollmeier, P. G.; Brylak, M. *Z. Naturforsch. B* **1997**, *52*, 560−564.

(12) Nientiedt, A. T.; Jeitschko, W. *Inorg. Chem.* **1998**, *37*, 386−389.

(13) Ding, C.; Man, H.; Qin, C.; Lu, J.; Sun, Y.; Wang, Q.; Yu, B.; Feng, C.; Goko, T.; Arguello, C. J.; Liu, L.; Frandsen, B. J.; Uemura, Y. J.; Wang, H.; Luetkens, H.; Morenzoni, E.; Han, W.; Jin, C. Q.; Munsie, T.; Williams, T. J.; D'Ortenzio, R. M.; Medina, T.; Luke, G. M.; Imai, T.; Ning, F. L. *Phys. Rev. B* **2013**, *88*, 041102(R).

(14) Li, X.; Wu, X.; Yang, J. *J. Mater. Chem. C* **2013**, *1*, 7197−7201.

(15) Perdew, J. P.; Burke, K.; Ernzerhof, M. *Phys. Rev. Lett.* **1996**, *77*, 3865−3868.

(16) Kresse, G.; Furthmüller, J. *Phys. Rev. B* **1996**, *54*, 11169−11186.

(17) Liechtenstein, A. I.; Anisimov, V. I.; Zaane, J. *Phys. Rev. B* **1995**, *52*, 5467−5470.

(18) Okabayashi, J.; Kimura, A.; Rader, O.; Mizokawa, T.; Fujimori, A.; Hayashi, T.; Tanaka, M. *Phys. Rev. B* **1998**, *58*, R4211−R4214.

(19) Mizokawa, T.; Fujimori, A. *Phys. Rev. B* **1993**, *48*, 14150−14156.

(20) Wierzbowska, M.; Sánchez-Portal, D.; Sanvito, S. *Phys. Rev. B* **2004**, *70*, 235209.

(21) Sato, K.; Dederichs, P. H.; Katayama-Yoshida, H.; Kudrnovský, J. *J. Phys.: Condens. Matter* **2004**, *16*, S5491−S5497.

(22) Larson, P.; Lambrecht, W. R. L.; Chantis, A.; Schilfgaarde, M. *Phys. Rev. B* **2007**, *75*, 045114.
(23) Blöchl, P. E. *Phys. Rev. B* **1994**, *50*, 17953−17979.
(24) Kayanuma, K.; Hiramatsu, H.; Kamiya, T.; Hirano, M.; Hosono, H. *J. Appl. Phys.* **2009**, *105*, 073903.
(25) Ramirez, A. P. *J. Phys.: Condens. Matter* **1997**, *9*, 8171−8199.
(26) Urushibara, A.; Moritomo, Y.; Arima, T.; Asamitsu, A.; Kido, G.; Tokura, Y. *Phys. Rev. B* **1995**, *51*, 14103−14109.
(27) Schiffer, P.; Ramirez, A. P.; Bao, W.; Cheong, S. W. *Phys. Rev. Lett.* **1995**, *75*, 3336−3339.
(28) Iimura, S.; Matuishi, S.; Sato, H.; Hanna, T.; Muraba, Y.; Kim, S. W.; Kim, J. E.; Takata, M.; Hosono, H. *Nat. Commun.* **2012**, *3*, 943.
(29) Hanna, T.; Matsuishi, S.; Kodama, K.; Otomo, T.; Shamoto, S.; Hosono, H. *Phys. Rev. B* **2013**, *87*, 020401(R).
(30) de la Cruz, C.; Huang, Q.; Lynn, J. W.; Li, J.; Ratcliff, W.; Zarestky, J. L.; Mook, H. A.; Chen, G. F.; Luo, J. L.; Wang, N. L.; Dai, P. *Nature* **2008**, *453*, 899−902.
(31) Emery, N.; Wildman, E. J.; Skakle, J. M. S.; Giriat, G.; Smith, R. I.; Mclaughlin, A. C. *Chem. Commun.* **2010**, *46*, 6777−6779.
(32) Yanagi, H.; Watanabe, T.; Kodama, K.; Iikubo, S.; Shamoto, S.; Kamiya, T.; Hirano, M.; Hosono, H. *J. Appl. Phys.* **2009**, *105*, 093916.
(33) Zhou, J.; Sun, Q. *J. Am. Chem. Soc.* **2011**, *133*, 15113−15119.
(34) Zhou, J.; Wang, Q.; Sun, Q.; Jena, P. *Phys. Rev. B* **2011**, *84*, 081402(R).
(35) Xiang, H. J.; Wei, S. H.; Whangbo, M. H. *Phys. Rev. Lett.* **2008**, *100*, 167207.
(36) Heyd, J.; Scuseria, G. E.; Ernzerhof, M. *J. Chem. Phys.* **2003**, *118*, 8207−8215.
(37) Heyd, J.; Scuseria, G. E.; Ernzerhof, M. *J. Chem. Phys.* **2006**, *124*, 219906.
(38) Dietl, T.; Ohno, H.; Matsukura, F.; Cibert, J.; Ferrand, D. *Science* **2000**, *287*, 1019−1022.
(39) Jungwirth, T.; König, J.; Sinova, J.; Kučera, J.; MacDonald, A. H. *Phys. Rev. B* **2002**, *66*, 012402.
(40) Henkelman, G.; Arnaldsson, A.; Jónsson, H. *Comput. Mater. Sci.* **2006**, *36*, 254−360.
(41) Pick, Š.; Dreyssé, H. *Phys. Rev. B* **1993**, *48*, 13588−13595.
(42) Wang, D. S.; Wu, R.; Freeman, A. J. *Phys. Rev. B* **1993**, *47*, 14932−14947.
(43) Daalderop, G. H. O.; Kelly, P. J.; Schuurmans, M. F. H.; Jansen, H. J. F. *J. Phys. Colloques* **1988**, *49*, C8−93-C8−94.
(44) Daalderop, G. H. O.; Kelly, P. J.; Schuurmans, M. F. H. *Phys. Rev. B* **1990**, *41*, 11919−11937.
(45) Moulas, G.; Lehnert, A.; Rusponi, S.; Zabloudil, J.; Etz, C.; Ouazi, S.; Etzkorn, M.; Bencok, P.; Gambardella, P.; Weinberger, P.; Brune, H. *Phys. Rev. B* **2008**, *78*, 214424.
(46) Lehnert, A.; Dennler, S.; Błoński, P.; Rusponi, S.; Etzkorn, M.; Moulas, G.; Bencok, P.; Gambardella, P.; Brune, H.; Hafner, J. *Phys. Rev. B* **2010**, *82*, 094409.
(47) Kan, E.; Hu, W.; Xiao, C.; Lu, R.; Deng, K.; Yang, J.; Su, H. *J. Am. Chem. Soc.* **2012**, *134*, 5718−5721.